An electromagnetic shashlik calorimeter with longitudinal segmentation

A.C. Benvenuti[a], I. Britvich[b], T. Camporesi[c],*, P. Checchia[d], A. Feniouk[b], V. Hedberg[e], V. Lishin[b], M. Margoni[d], M. Mazzucato[d], V. Obraztsov[b], M. Paganoni[f], V. Poliakov[b], F. Simonetto[d], F. Terranova[f], E. Vlasov[b]

[a]*Dipartimento di Fisica, Università di Bologna and INFN, Bologna, Italy*
[b]*Institute for High Energy Physics, Serpukov, Russia*
[c]*CERN, European Organization for Nuclear Research, 1211 Geneva 23, Switzerland*
[d]*Dipartimento di Fisica, Università di Padova and INFN, Padua, Italy*
[e]*Department of Physics, University of Lund, Lund, Sweden*
[f]*Dipartimento di Fisica, Università di Milano and INFN, Milan, Italy*

Abstract

A novel technique for longitudinal segmentation of shashlik calorimeters has been tested in the CERN West Area beam facility. A 25 tower very fine samplings e.m. calorimeter has been built with vacuum photodiodes inserted in the first 8 radiation lengths to sample the initial development of the shower. Results concerning energy resolution, impact point reconstruction and e/π separation are reported. © 1999 Elsevier Science B.V. All rights reserved.

1. Introduction

In recent years the "shashlik" technology has been extensively studied to assess its performance at e^+e^-, ep and pp accelerator experiments [1–4]. Shashlik calorimeters are sampling calorimeters in which scintillation light is read-out via wavelength shifting (WLS) fibers running perpendicularly to the converter/absorber plates [5,6]. This technique offers the combination of an easy assembly, good hermeticity and fast time response. In many applications it also represents a cheap solution compared to crystals or cryogenic liquid calorimeters.

Shashlik calorimeters are, in particular, considered to be good candidates for barrel electromagnetic calorimetry at future linear e^+e^- colliders [7]. In this context, the physics requirements impose $\sigma(E)/E \leq 0.1/\sqrt{E(\text{GeV})} + 0.01$, at least three longitudinal samplings, transversal segmentation of the order of $0.9° \times 0.9°$ ($\sim 3 \times 3$ cm^2) and the possibility of performing the read-out in a 3 T magnetic field. The present shashlik technology can satisfy these requirements, except for the optimization of longitudinal segmentation which still needs development. The solution proposed in this paper consists of thin vacuum photodiodes inserted between adjacent towers in the front part of the calorimeter. They measure the energy deposited in the initial shower development that allows for longitudinal sampling and e/π separation. A prototype

---

* Corresponding author. Tel.: + 41-22-767-26-77; fax: + 41-22-782-3084.

E-mail address: tiziano.camporesi@cern.ch (T. Camporesi)

detector was exposed to a beam with the aim of measuring the sampling capability and demonstrating that the insertion of diodes neither deteriorates critically the energy response nor produces significant cracks in the tower structure.

2. The prototype detector

The tested prototype had 25 Pb/scintillator towers, assembled in a 5×5 matrix. Each tower consisted of 140 layers of 1 mm thick lead and 1 mm thick scintillator tiles, resulting in a total depth of $25X_0$. The sampling was the finest ever used with the shashlik technique. The transversal dimension of each tower was 5×5 cm^2. In the first $8X_0$ the tiles had a smaller transverse dimension to provide room for the housing of the diodes. Plastic scintillator consisting of polystyrene doped with 1.5% paraterphenyl and 0.05% POPOP was used. Optical insulation between the towers was provided by white Tyvek paper.

As it is customary in shashlik technique, the blue light produced in the scintillator was carried to the photodetector at the back of the calorimeter by means of plastic optical fibers doped with green WLS. The 1 mm diameter fibers crossed the tiles in holes drilled in the lead and scintillator plates and they were uniformly distributed with a density of 1 fiber/cm^2. In the scintillator tiles the holes were 3 mm in diameter (4 mm in the lead). The light transmission between the plastic scintillator and the fibers was in air. All the fibers from the same tower were bundled together at the back and connected to photodetectors. Two types of fibers were tested: Bicron BCF20 fibers and Kuraray Y11. In both cases, the emission peak was at about 500 nm. Light collection was increased by aluminizing the fiber end opposite to the photodetector by sputtering.

The light from the fibers was viewed after a 5 mm air gap by 1 "Hamamatsu R2149-03 phototetrodes. Each tetrode was placed inside an aluminum housing, containing a charge sensitive JFET preamplifier and a high-voltage divider. The differential output signals were shaped with a shaping time of 1.500 µs and digitized. Four towers were read-out with Hamamatsu Avalanche Photodiodes instead

of tetrodes. A plexiglass light guide was used to match the smaller APD sensitive area to the fiber bundle. Preamplifiers and voltage dividers were housed in the same mechanical structure as the tetrodes.

Two types of vacuum photodiodes, viewed with a bialkali photocathode, were produced by EMI[1] (Hamamatsu[2]) with a rectangular (squared) front surface of 9×5 cm^2 (5×5 cm^2) and a thickness of 5 mm. The diodes were installed in the first part of the towers in order to sample the energy deposited in the first $8X_0$. They were in optical contact with the lateral side of the scintillator tiles and the light emitted in the first part of the detector was therefore read-out twice since the photons crossing the lateral scintillator surface were collected by the diode while those reaching the fibers, either directly or after reflections, were seen by the tetrodes. Due to the direct coupling, the light collection efficiency of the diodes was much larger than that of the tetrodes/APDs and this compensated for the absence of gain in the diodes.

Most of the cells were equipped with EMI vacuum photodiodes. One diode prototype from Hamamatsu, sampling only $4X_0$, was successfully tested during the last part of the data taking. Technical characteristics of these devices are listed in Table 1. The Hamamatsu prototype dimensions are such that it is possible to house two diodes in the same tower in order to obtain three longitudinal samplings. For all diodes, the same front-end electronics and read-out chain as for the tetrodes were used. The read-out electronics was positioned above the tower stacks (see Fig. 1).

3. Testbeam setup

The prototype was tested at the X5 beam in the CERN West Area. Electrons ranging from 5 to 75 GeV and pions of 20, 30 and 50 GeV were used. The prototype (CALO in Fig. 2) was installed on a moving platform whose position was controlled at the level of $\simeq 220$ µm. In order to avoid

---

[1] EMI vacuum photodiode prototype D437.

[2] Hamamatsu vacuum photodiode prototype SPTXC0046.

Table 1
Technical characteristics of vacuum photodiodes

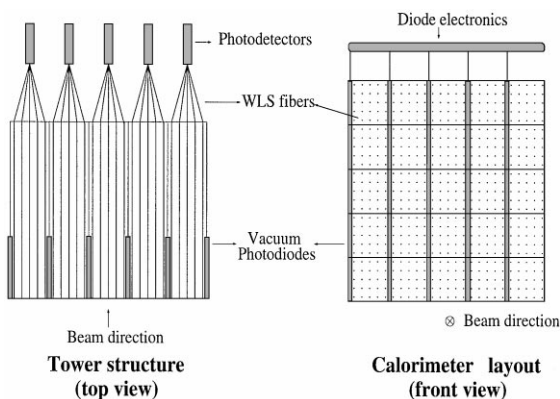|	EMI	Hamamatsu
Sensitive area	28.9 cm^2	10.9 cm^2
Diode thickness	5.0 mm	5.1 mm
Working bias	− 10 V	− 20 V
Capacitance	250 pF	17 pF
Energy equivalent e.noise	∼ 1200 MeV	∼ 900 MeV

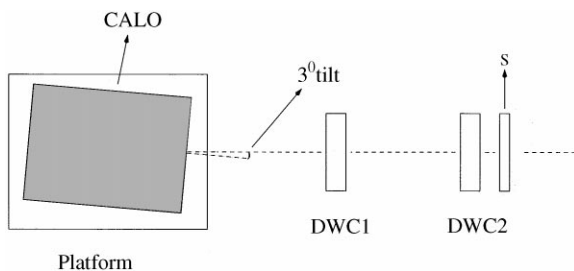Fig. 1. Layout of the calorimeter prototype (not in scale).

Fig. 2. Top view of the testbeam setup (not in scale). "CALO" is the calorimeter tilted by 3° with respect to the beam direction, "DWC1"-"DWC2" are the Delay Wire Chambers and "S" the scintillator telescope.

particles from channeling through fibers or diodes, the calorimeter was tilted by 3° in the horizontal plane with respect to the beam direction. The absolute impact position of the incoming particle was measured by means of two Delay Wire Chambers

(DWC1 and DWC2) with a 2 mm wire pitch and a spatial resolution of 200 μm, positioned at 0.5 and 1 m from the calorimeter frontface. External trigger was provided by a layer of scintillators installed near DWC2.

A calibration of each tower was carried out by exposing the calorimeter to a 50 GeV electron beam at the beginning of each of the two data taking periods. The diode signals were calibrated with 50 GeV electrons as well. Pedestal runs were taken periodically to monitor the noise of the electronic amplification chain.

4. Results

4.1. Energy resolution

The energy response is expected to depend on the impact point since the nearer the fiber the higher the light collection efficiency. The high fiber density was used in order to reduce the non uniformity in light response to a level of a few percent. This effect was, however, not achieved with BCF20 fibers, due to a small scintillating component deteriorating the energy resolution. KY11 fibers, on the other hand, had a non-uniformity at the level of ± 1.5%. Fig. 3 shows the energy response for 50 GeV electrons in towers equipped with Kuraray fibers and tetrode read-out. The energy resolution achieved with KY11 fibers and tetrode read-out as a function of the beam energy is shown in Fig. 4 and can be parameterized as[3]

$$\frac{\sigma(E)}{E} = \sqrt{\left(\frac{9.6\%}{\sqrt{E}} + 0.5\%\right)^2 + \left(\frac{0.130}{E}\right)^2} \qquad (1)$$

where E is expressed in GeV. The last term corresponds to the electronic noise contribution and was measured from pedestal runs. A Geant Monte Carlo simulation of the shower development in a 1-mm-lead/1-mm-scintillator sampling gave a

---

[3] Alternatively, by adding the constant term in quadrature:

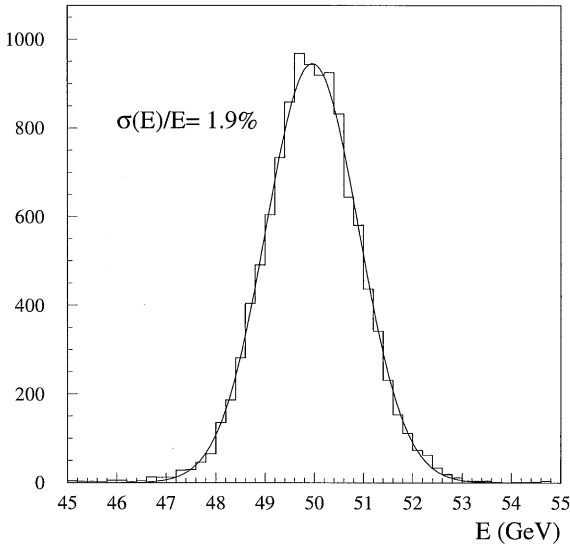$$\frac{\sigma(E)}{E} = \frac{10.1\%}{\sqrt{E}} \oplus 1.3\% \oplus \frac{0.130}{E}.$$

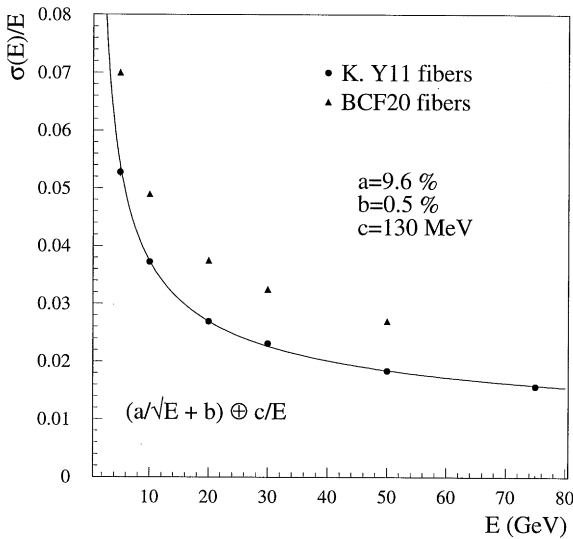Fig. 3. Energy resolution for 50 GeV electrons using tetrode read-out and KY11 optical fibers.

Fig. 4. Relative energy resolution versus electron beam energy using tetrode read-out and KY11 optical fibers. The values obtained using the BCF20 fibers are also shown.

smaller value ($\sim 6\%/\sqrt{E}$) for the first term of the energy resolution. Therefore, the dominant contribution to the measured resolution was attributed to the photoelectron statistics.

The use of phototetrodes is not ideal for barrel calorimetry at e^+e^- colliders. Tetrodes have a rather long longitudinal dimension and must be kept at a small angle with respect to the magnetic field in order to operate with a maximum gain. The installation of Avalanche Photodiodes has been proposed by the CMS collaboration [8] as an alternative solution. Given their very good quantum efficiency ($\sim 80\%$), APD should also ensure a better energy resolution when the photoelectron statistics contribution dominates. Four APDs were installed in the prototype, as described in Section 2, but unfortunately, no towers were equipped with APD and KY11 fibers. In Fig. 5 the energy response for 50 GeV electrons impinging on a tower equipped with APD is shown. The high-energy tail coming from events reconstructed near the BCF20 fibers is evident.

4.2. Linearity

Fig. 6 shows the reconstructed energy versus the nominal electron beam energy when the beam was centered in towers equipped with KY11 fibers. No significant deviations from linearity were observed up to 75 GeV which was the highest energy measured.
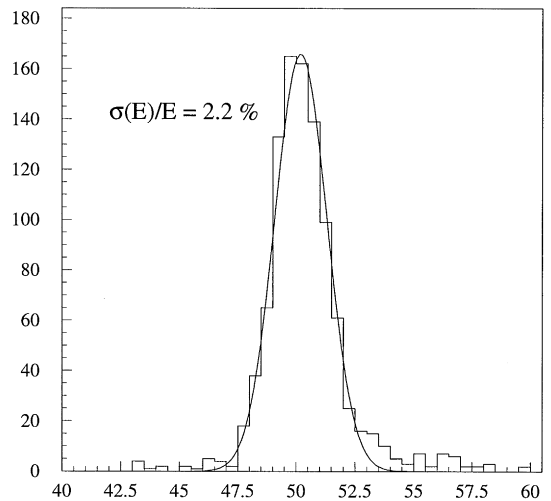

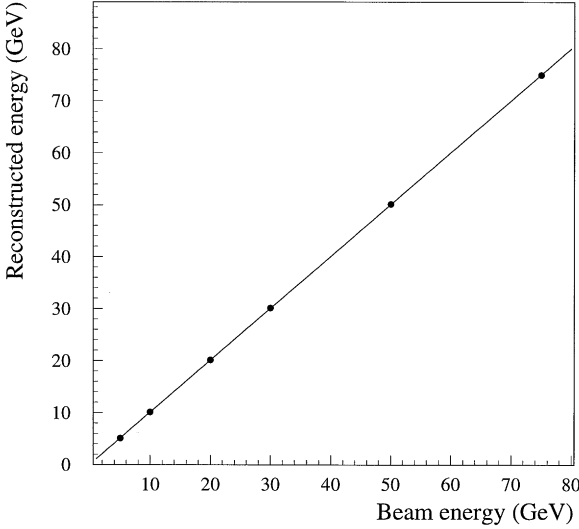Fig. 5. Energy resolution for 50 GeV electrons using an APD as photodetector.

Fig. 6. Energy reconstructed using the calibration coefficients computed at 50 GeV versus nominal e⁻ beam energy.

4.3. Spatial resolution

A position scan along the towers was done using 50 GeV electrons to establish the precision in the impact point reconstruction. The shower position reconstruction was based on the center of gravity method corrected for the detector granularity with the algorithm suggested by Akopdjanov et al. [9]. The barycenter

$$X_b = 2\Delta \sum_i iE_i \Big/ \sum_i E_i. \tag{2}$$

(Δ is the half-width of the tower and E_i the energy deposited in tower i), was modified according to

$$X_c = b \, \text{arcsinh}\left(\frac{X_b}{\Delta} \sinh \delta\right) \tag{3}$$

where b is a parameter describing the transversal shower profile and $\delta \equiv \Delta/b$. Since the shower profile was not described by a single exponential, a two steps procedure was followed: in the first step X'_c was determined with $b = 0.85$ cm and in the second one the value of b was recomputed in the interval $0.45 < b < 0.85$ according to X'_c. X_c was linear in most of the impact point range, showing non-linearities only near the diode housing as depicted in Fig. 7. The non-linear behavior around

the diode was corrected for by using the diode signal itself. In particular, in the range of X_c close to the distortion region, a diode-based estimator was introduced so that

$$X' = X_c + X_d \tag{4}$$

where

$$X_d = -b' \log \frac{1}{2}\left(1 + \frac{E_{\text{diode}}^{\text{max}}}{E^{\text{max}+1}}\right) + c' \tag{5}$$

here $E_{\text{diode}}^{\text{max}}$ is the diode energy in the tower with maximum signal, $E^{\text{max}+1}$ represents the energy (seen by tetrodes/APDs) in the tower closest to the reconstructed impact position and the parameters b' and c' were determined with 50 GeV electrons and are $b' = 0.2$ cm and $c' = 0.3$ cm.

The position resolution of the prototype at the cell center was 1.6 mm with 50 GeV electrons and had the following energy dependence:

$$\sigma_X(E) = \sqrt{\left(\frac{0.9}{\sqrt{E}}\right)^2 + (0.1)^2} \text{cm}. \tag{6}$$

4.4. Energy leakage to the diode

The dead zone between two adjacent towers due to the diode affected only a limited portion of the
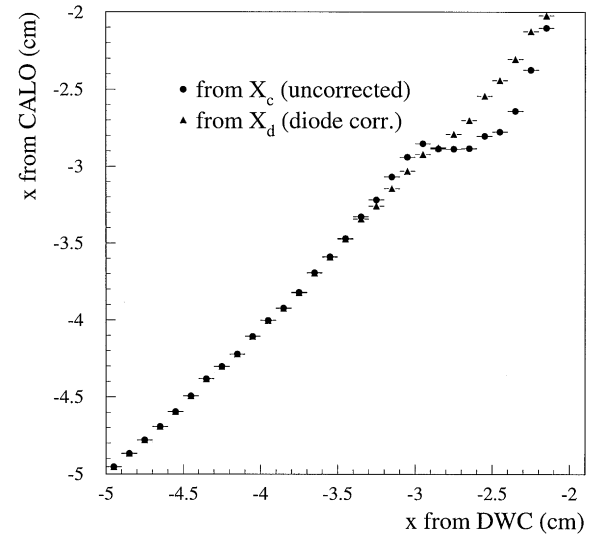

Fig. 7. Reconstructed horizontal impact position versus beam one (from DWC). X_c was estimated with Eq. (3) and X_d with Eq. (4).

calorimeter and was always followed by a sufficiently long ($> 15X_0$) part of the active detector. Therefore, no complete cracks existed in the calorimeter. Nevertheless, an energy loss for showers developing near the diode was visible. It was easily corrected for by using the reconstructed shower impact point. The energy response as a function of the distance y of the reconstructed position from the two tower border was parametrized as

$$E(y) = E_0 \cdot (1 - a e^{-y^2/2\sigma_{\pm}^2}) \tag{7}$$

where $a = 0.075$, $\sigma_+ = 0.45$ cm for $y > 0$ and $\sigma_- = 1.19$ cm for $y < 0$. Fig. 8 shows the energy response, before and after the correction, as a function of the reconstructed position for 50 GeV electrons. Once the correction was introduced, the remaining non-uniformity in the energy response was due to the difference in light collection near fibers.

4.5. Diode response

The EMI and the Hamamatsu diode responses to 50 GeV electrons and pions are shown in Fig. 9. The widths of both distributions were dominated by the fluctuations in the shower development. Due
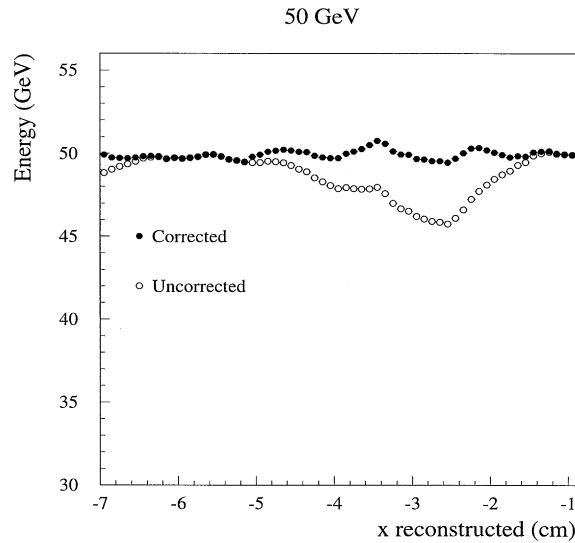

Fig. 9. Energy response for 50 GeV electrons (black dots) and pions (line) for EMI and Hamamatsu diode prototypes.

Fig. 8. Energy versus reconstructed horizontal impact position before (open circles) and after (black dots) correction.
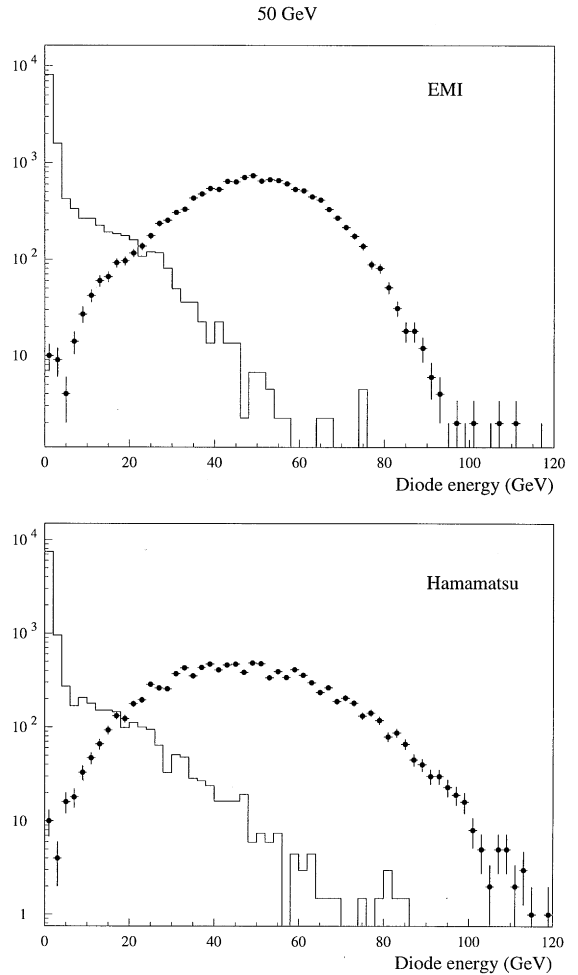
to the different sampling seen by the two detectors, the light signal was larger for the EMI and the fluctuations were more important in the case of the Hamamatsu prototype. On the other hand, the smaller capacitance of the latter ensured a much lower electronic noise giving a comparable energy equivalent contribution as indicated in Table 1.

Since the showers were not contained in the part of the calorimeter read-out by diodes and the longitudinal shower development depends on the energy, the response at different electron energies was not linear as shown in Fig. 10.

4.6. e/π separation

Separation of electrons from pions was performed using discriminating variables based either on purely calorimetric data or involving also ex-

Fig. 10. Energy response using the calibration coefficients computed at 50 GeV versus nominal electron beam energy (EMI diode).

ternal information like the beam energy, known from the settings of main deflection magnet, which would be replaced by the momentum estimation from the tracking in a collider experiment. The fraction

$$\chi_E = \frac{E_{cal}}{E_{beam}} \tag{8}$$

can be combined with pure calorimeter variables like the fraction of energy seen by the diodes

$$\chi_D = \frac{E_{diode}}{E_{cal}} \tag{9}$$

and the lateral development of the shower

$$\chi_S = \frac{\sum_{i=1}^{N} E_i r_i^2}{\sum_{i=1}^{N} E_i} \tag{10}$$

where N is the number of towers with signal and r_i the distance of the tower from the reconstructed impact position.

Fig. 11 shows E_{diode} versus E_{cal} for pions and electrons at 20 GeV. The discriminating power of the different variables in terms of pion contamination for 90% electron efficiency, at energies ranging from 20 to 50 GeV is shown in Fig. 12. In most of the cases, purely calorimetric variables improve the
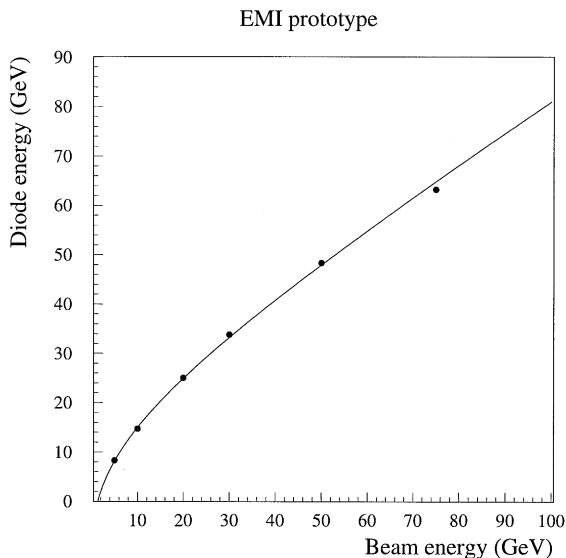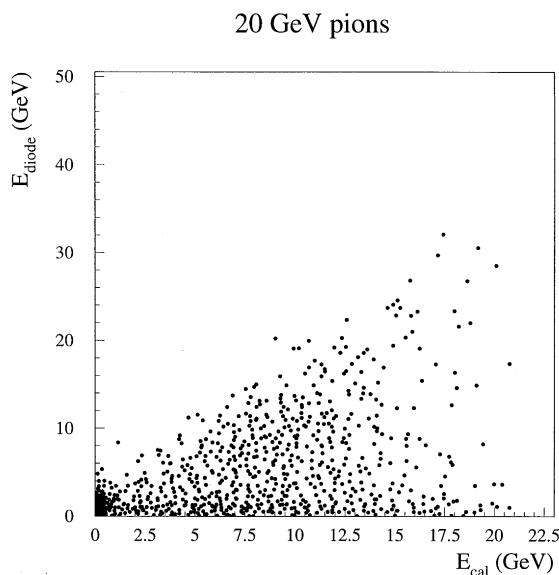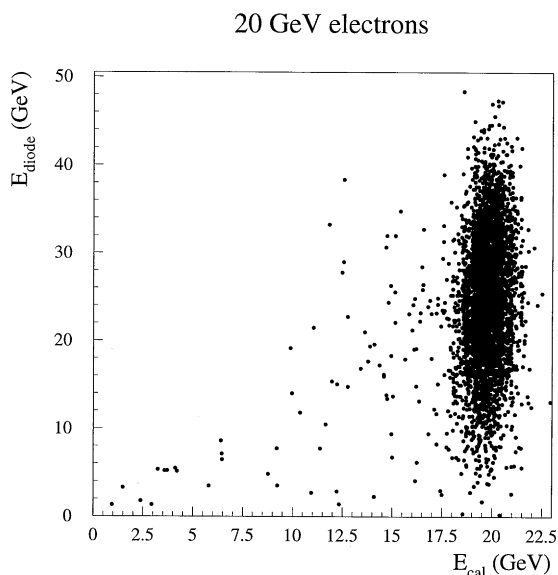

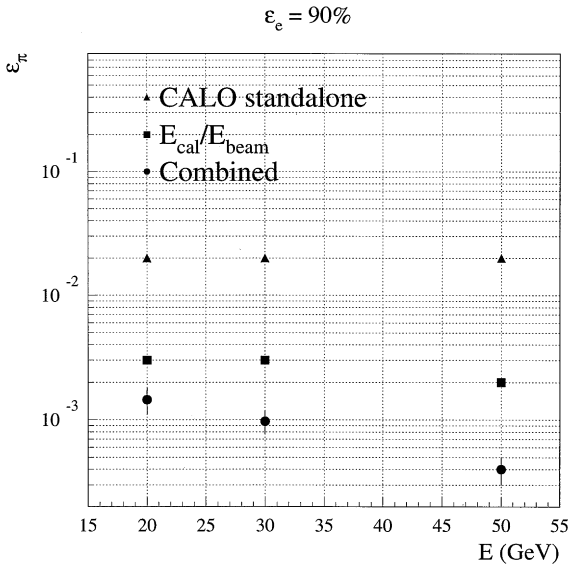Fig. 11. Diode energy versus total tetrode energy for e and π at 20 GeV.

Fig. 12. Pion contamination versus energy for 90% electron efficiency.

overall separation capability with a factor ~ 2 compared with χ_E by itself. At 50 GeV the pion contamination for 90% electron efficiency is $(4.0 \pm 1.5) \times 10^{-4}$.

5. Conclusions

The present test has demonstrated the technical feasibility of longitudinally segmented shashlik calorimeters in which lateral sampling is performed by vacuum photodiodes. Due to the small dimension of the diodes and to the tilt of fibers and diodes with respect to the incoming particles, no significant cracks or dead zones are introduced. Performance in terms of energy resolution, impact point reconstruction and e/π separation seem to be adequate for applications at future e^+e^- collider experiments.

Acknowledgements

References

[1] J. Badier et al., Nucl. Instr. and Meth. A 348 (1994) 74.
[2] HERA-B Design Report, DESY/PRC 95-01.
[3] LHCb Technical Proposal, CERN/LHCC 98-4.
[4] S.J. Alsvaag et al., CERN/EP 98–132.
[5] H. Fessler et al., Nucl. Instr. and Meth. A 240 (1985) 284.
[6] G.S. Atoyan et al., Nucl. Instr. and Meth. A 320 (1992) 144.
[7] R. Brinkmann, G. Materlik, J. Rossbach, A. Wagner (Eds.), DESY 1997-048.
[8] CMS Technical Proposal, CERN/LHCC 94-38.
[9] G.A. Akopdjanov et al., Nucl. Instr. and Meth. 140 (1977) 441.